Journal of Magnetic Resonance **156,** 213–221 (2002)
doi:10.1006/jmre.2002.2550

# Modelling of Self-diffusion and Relaxation Time NMR in Multicompartment Systems with Cylindrical Geometry

Louise van der Weerd,*,[1] Sergey M. Melnikov,† Frank J. Vergeldt,* Eugene G. Novikov,† and Henk Van As*,[2]

*Laboratory of Biophysics, Wageningen University, Wageningen, The Netherlands; and †Department of Systems Analysis, Belarusian State University, Minsk, Belarus

Received October 30, 2001; revised April 23, 2002

**Multicompartment characteristics of relaxation and diffusion in a model for (plant) cells and tissues have been simulated as a means to test separating the signal into a set of these compartments. A numerical model of restricted diffusion and magnetization relaxation behavior in PFG-CPMG NMR experiments, based on Fick's second law of diffusion, has been extended for two-dimensional diffusion in systems with concentric cylindrical compartments separated by permeable walls. This model is applicable to a wide range of (cellular) systems and allows the exploration of temporal and spatial behavior of the magnetization with and without the influence of gradient pulses. Numerical simulations have been performed to show the correspondence between the obtained results and previously reported studies and to investigate the behavior of the apparent diffusion coefficients for the multicompartment systems with planar and cylindrical geometry. The results clearly demonstrate the importance of modelling two-dimensional diffusion in relation to the effect of restrictions, permeability of the membranes, and the bulk relaxation within the compartments. In addition, the consequences of analysis by multiexponential curve fitting are investigated.** 

*Key Words*: **NMR; restricted diffusion; relaxation; numerical modelling; Fick's second law of diffusion.**

## INTRODUCTION

Both pulsed field gradient NMR and relaxation time measurements are widely used to probe the molecular displacements of liquid molecules and the geometry of the microstructures containing them in porous and biological media (*1–4*). In such systems the measured displacements and observed relaxation times contain information about the diffusivity within the compartments, the dimensions of the compartments, and the exchange between these compartments through semipermeable membranes (*5–14*). If diffusion takes place in compartments separated by permeable membranes, as is the situation for most biological cells, the membrane permeability and differences in (bulk) relaxation times within the compartments strongly affect the shape of the signal attenuation plot (SAP) or the q-dependence and thus the apparent diffusion coefficient $D^*$. Especially the effect of differences in bulk relaxation in combination with membrane permeabilities on $D^*$ has hardly been taken into consideration in literature, but clearly cannot be ignored (*2, 9, 11, 14*).

Combined diffusion and relaxation time measurements and analysis, also called diffusion analysis by relaxation time separation (DARTS) (*5, 13*), yield more detailed insight in the behavior of the different liquid ensembles and the microstructure (*10, 12, 15–18*). However, for further improvement of the experimental setup and analysis approach, and for a better understanding of the complex molecular behavior, we require adequate mathematical models to evaluate the effect of diffusion and relaxation on the observed NMR signal.

Among the broad spectrum of the reported modelling approaches, three ways are clearly distinguishable. The first approach is an analytical solution of the given partial differential equation for a certain combination of the initial and boundary conditions (*11, 19*). Despite the fact that solutions in a closed analytical form are obtained, the number of analytically treated configurations is limited. Another approach consists of the detailed reproduction of every molecular movement and transformation using simulation methods (*20, 21*). The position and orientation of every spin should be calculated for every time step, thus allowing the most extraordinary system configurations, but software implementation of such procedures may be very time-consuming even for simple configurations on powerful workstations. The compromised way of action is based on the numerical solution of the partial differential equation with respect to spin magnetization (*6, 9, 14*). This approach ensures, on the one hand, reasonable speed of calculations and, on the other hand, the possibility to investigate rather complicated configurations. These models are generally based on the different evaluations of Fick's second law of diffusion (*22*). In this way, a variety of systems with complicated configurations can be modelled by simply defining appropriate initial and boundary conditions, combined with a proper description of the shape of the pulsed magnetic field gradients (*11, 19*). This approach is adopted for the model presented in this paper.

[1] Present address: Royal College of Surgeons, Unit of Biophysics, Institute of Child Health, London, UK.

[2] To whom correspondence should be addressed. E-mail: henk.vanas@water.mf.wau.nl.



1090-7807/02 $35.00

Previously, we reported a numerical model to simulate the combined diffusion and magnetization relaxation behavior in NMR experiments for planar geometries (*9*). However, more realistic models should, of course, take into account the (concentric) cylindrical symmetry of many biological objects. Doing so, the effect of restricted diffusion and the possibility to circumvent a diffusion barrier by two-dimensional diffusion can be investigated. Examples of such a concentric cylindrical geometry are plant xylem vessels and blood vessels surrounded by cellular tissues, and vacuolized plant cells, in which a large inner compartment, the vacuole, is surrounded by two thin layers, the cytoplasm and cell wall. All compartments have distinct relaxation and diffusion properties and diffusional exchange between these compartments can occur (*22, 23*). In this paper we demonstrate the agreement of the obtained results with results that were reported previously for cylindrical geometries and we show examples of typical differences between planar and cylindrical geometries. This approach may be of great value to understand the complicated process of exchange in biological and porous structures and is a stepstone towards even more realistic, and hence more complicated, models. Such models are necessary to understand the relation between microanatomical structure of tissues and the origin and variation of image contrast in MRI. In addition, we need such models to solve the question of how far (and in what way) combined diffusion-relaxation time measurements allow us to separate signals into a set of multicompartmental sources.

## THEORY

A two-dimensional system is considered that consists of a set of concentric cylindrical compartments, each surrounded by a membrane (Fig. 1). The $i$th compartment is characterized by an intrinsic relaxation time $T_j$ and diffusion constant $D_j$ as well as by a radius $R_j$ and permeability $\rho_{j-1}$ and $\rho_j$ for the inner and outer membrane, except for the innermost compartment where only an outer membrane is present.

The two-dimensional spin magnetisation density $S(r, \varphi, t)$ can be described in cylindrical coordinates by the following differential equation based on Fick's second law of diffusion, including the effect of relaxation (*22*),

$$\frac{\partial S(r,\varphi,t)}{\partial t} = \frac{\partial}{r\partial r}\left\{r\,D(r,\varphi)\frac{\partial S(r,\varphi,t)}{\partial r}\right\} + \frac{\partial}{r^2\partial\varphi}\left\{D(r,\varphi)\frac{\partial S(r,\varphi,t)}{\partial\varphi}\right\} - \frac{S(r,\varphi,t)}{T(r,\varphi)}, \quad [1]$$

where $D(r, \varphi)$ and $T(r, \varphi)$ are the diffusion coefficient and relaxation time, respectively, as a function of the radius and angle. Diffusion and relaxation are assumed to be constant within a particular compartment, but may differ for different compartments. Equation [1] should be supplemented by a proper set of initial and boundary conditions. Magnetization at time $t = 0$ takes the form

$$S(r, \varphi, t)_{t=0} = f(r, \varphi), \quad [2]$$

where $f(r, \varphi)$ is the spin magnetization density at time $t = 0$. The permeability $\rho$ of the membranes is accounted for by boundary conditions in two dimensions and is formulated analogously to the one-dimensional case (*9*). For the internal and external membranes of the $j$th compartment, one can then write

$$\begin{aligned} &\rho_{j-1}[S_j(R_{j-1},\varphi,t) - S_{j-1}(R_{j-1},\varphi,t)] \\ &\quad = D(R_{j-1},\varphi)\frac{\partial S_j(R_{j-1},\varphi,t)}{\partial r}, \\ &\rho_j[S_{j+1}(R_j,\varphi,t) - S_j(R_j,\varphi,t)] \\ &\quad = D(R_j,\varphi)\frac{\partial S_j(R_j,\varphi,t)}{\partial r}, \end{aligned} \quad [3]$$

where $S_j(r, \varphi, t) = S(r, \varphi, t)$, when $r \in [R_{j-1}, R_j], j = 1, \ldots, n$,

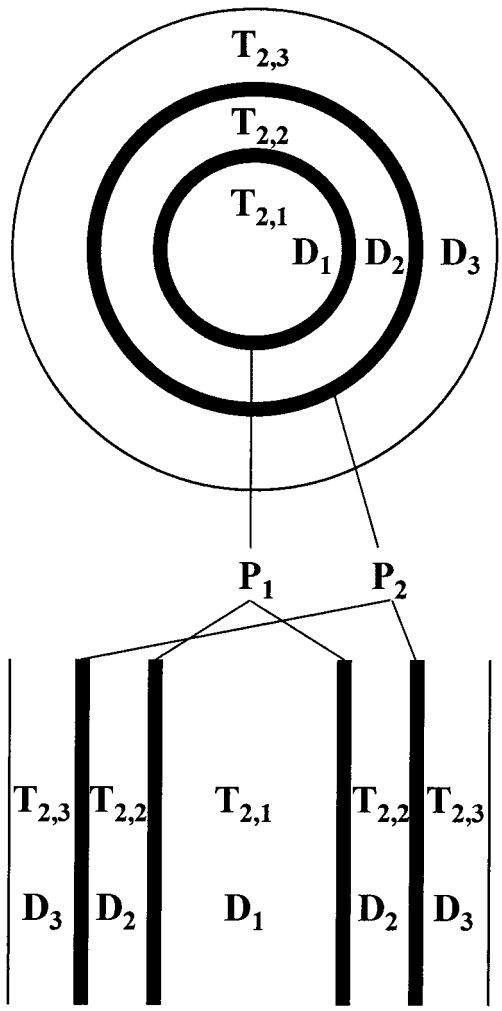


**FIG. 1.** Structure of multicompartment systems with cylindrical and planar geometries.

$R_0 = 0$, and $n$ is the number of compartments. The outer border of the system is characterized by

$$S_{n+1}(R_n, \varphi, t) = F(t), \qquad [4]$$

where $F(t)$ is the outer spin magnetization at time step $t$.

The numerical solution of Eq. [1] with the initial condition Eq. [2] and boundary conditions Eq. [3] is based on the transformation of Eq. [1] to an equation in finite differences according to an implicit scheme (*24*),

$$\begin{aligned} S_{p,q}^{m+1/2} &= S_{p,q}^{m} + \frac{\Delta t}{2}\left(\phi_r^2 S_{p,q}^{m+1/2} + \phi_\varphi^2 S_{p,q}^{m}\right) - \frac{\Delta t S_{p,q}^{m+1/2}}{2T_{p,q}}, \\ S_{p,q}^{m+1} &= S_{p,q}^{m+1/2} + \frac{\Delta t}{2}\left(\phi_r^2 S_{p,q}^{m+1/2} + \phi_\varphi^2 S_{p,q}^{m+1}\right) - \frac{\Delta t S_{p,q}^{m+1}}{2T_{p,q}}, \end{aligned} \qquad [5]$$

where $S_{p,q}^{m} = S(r_p, \varphi_q, t_m)$, and the indexes $m$, $p$, and $q$ denote time step, radius step, and angle step, respectively; $\phi_r^2$ and $\phi_\varphi^2$ are the finite differences of the second order with respect to radius and angle, respectively. The finite difference scheme of Eq. [5] shows how spin magnetization density at the next time step $S_{p,q}^{m+1} = S(r_p, \varphi_q, t_m + \Delta t)$ is calculated from the spin magnetization density at the previous time step $S_{p,q}^{m} = S(r_p, \varphi_q, t_m)$ via spin magnetization density at half of the next time step $S_{p,q}^{m+1/2} = S(r_p, \varphi_q, t_m + \Delta t/2)$.

Assuming that the diffusion coefficient is independent on the angle ($D(r, \varphi) = D(r)$), the radial finite difference $\phi_r^2 S_{p,q}^{m}$ can be expressed as

$$\begin{aligned} \phi_r^2 S_{p,q}^{m} = \frac{1}{\Delta r^2}\Bigg\{ & D_{p+1/2}\left(1 + \frac{\Delta r}{2r_p}\right)\left(S_{p+1,q}^{m} - S_{p,q}^{m}\right) \\ & + D_{p-1/2}\left(1 - \frac{\Delta r}{2r_p}\right)\left(S_{p-1,q}^{m} - S_{p,q}^{m}\right)\Bigg\} \end{aligned} \qquad [6]$$

and for the angle finite difference $\varphi_\varphi^2 S_{p,q}^{m}$, one obtains

$$\phi_\varphi^2 S_{p,q}^{m} = \frac{D_p S_{p,q+1}^{m} - 2D_p S_{p,q}^{m} + D_p S_{p,q-1}^{m}}{r_r^2 \Delta\varphi^2}, \qquad [7]$$

where $D_p = D(r_p)$, and $\Delta r$ and $\Delta\phi$ are the radius and angle steps, respectively. The relaxation time $T(r, \varphi)$ is assumed to be independent of the angle $\varphi$: $T(r, \varphi) = T(r)$, $T_p = T(r_p)$. Substituting Eqs. [6] and [7] in Eq. [1] according to the numerical scheme of Eq. [5] yields after some transformations two sets of tridiagonal linear algebraic equations:

$$\begin{aligned} & \frac{\Delta t D_{p-1/2}}{2\Delta r^2}\left(1 - \frac{\Delta r}{2r_p}\right) S_{p-1,q}^{m+1/2} - \left\{\frac{\Delta t D_{p+1/2}}{2\Delta r^2}\left(1 + \frac{\Delta r}{2r_p}\right)\right. \\ & \quad \left. + \frac{\Delta t D_{p-1/2}}{2\Delta r^2}\left(1 - \frac{\Delta r}{2r_p}\right) + 1 + \frac{\Delta t}{2T_p}\right\} S_{p,q}^{m+1/2} \\ & \quad + \frac{\Delta t D_{p+1/2}}{2\Delta r^2}\left(1 + \frac{\Delta r}{2r_p}\right) S_{p+1,q}^{m+1/2} \\ & = -\frac{\Delta t D_p}{2r_r^2 \Delta\varphi^2} S_{p,q-1}^{m} + \left(\frac{\Delta t D_p}{r_r^2 \Delta\varphi^2} - 1\right) S_{p,q}^{m} - \frac{\Delta t D_p}{2r_r^2 \Delta\varphi^2} S_{p,q+1}^{m} \end{aligned} \qquad [8]$$

and

$$\begin{aligned} & \frac{\Delta t D_{p-1/2}}{2\Delta r^2}\left(1 - \frac{\Delta r}{2r_p}\right) S_{p-1,q}^{m+1/2} - \left\{\frac{\Delta t D_{p+1/2}}{2\Delta r^2}\left(1 + \frac{\Delta r}{2r_p}\right)\right. \\ & \quad \left. + \frac{\Delta t D_{p-1/2}}{2\Delta r^2}\left(1 - \frac{\Delta r}{2r_p}\right) - 1\right\} S_{p,q}^{m+1/2} \\ & \quad + \frac{\Delta t D_{p+1/2}}{2\Delta r^2}\left(1 + \frac{\Delta r}{2r_p}\right) S_{p+1,q}^{m+1/2} \\ & = -\frac{\Delta t D_p}{2r_r^2 \Delta\varphi^2} S_{p,q-1}^{m+1} + \left(\frac{\Delta t D_p}{r_r^2 \Delta\varphi^2} + 1 + \frac{\Delta t}{2T_p}\right) S_{p,q}^{m+1} \\ & \quad - \frac{\Delta t D_p}{2r_r^2 \Delta\varphi^2} S_{p,q+1}^{m+1}. \end{aligned} \qquad [9]$$

The solutions of the tridiagonal sets [8] and [9] can be obtained by the Gauss elimination method (*25*). Normally, it is supposed that the diffusion coefficient $D_p$ and the intrinsic relaxation time $T_p$ is constant within one compartment $D_{p-1/2} = D_{p+1/2} = D_p = D(r_p) = D_j$, $T_p = T(r_p) = T_j j$ when $r \in [R_{j-1}, R_j]$, $j = 1, \ldots, n$, and each membrane is treated as an additional compartment of the length $\Delta r$ with the diffusion coefficient $\rho_j \Delta r$ (*14*).

To account for the influence of magnetic field gradient pulses as used in PFG measurements, differential equation [1] takes the form (*25*)

$$\begin{aligned} \frac{\partial S(r, \varphi, t)}{\partial t} = & \frac{\partial}{r\partial t}\left\{ r D(r, \varphi) \frac{\partial S(r, \varphi, t)}{\partial r} \right\} \\ & + \frac{\partial}{r^2 \partial\varphi}\left\{ D(r, \varphi) \frac{\partial S(r, \varphi, t)}{\partial r} \right\} \\ & + \left( i\gamma g(t) r \cos(\varphi) - \frac{1}{T(r, \varphi)} \right) S(r, \varphi, t), \end{aligned} \qquad [10]$$

where $g(t)$ describes the sequence of magnetic field gradient pulses as a function of time, and $\gamma$ is the gyromagnetic ratio. In our case, $g(t)$ is a pair of magnetic field gradient pulses with the identical amplitude $G$, duration $\delta$, and opposite polarity; the distance between the leading edges of the gradient pulses is $\Delta$. The gradient pulses are applied along the polar axis direction (i.e., across a diameter). The finite difference scheme can be directly applied for the numerical solution of the differential equation (*24*). However, when the strength of the gradient pulses is high, the phase difference between adjacent positions can be very large and in that case it is impossible to get sufficient

accuracy with reasonable values for the time and space steps. In this case it is practicable to solve linear sets [8] and [9], assuming that there are no gradient pulses, and then perform the correction for the influence of the gradient pulses, multiplying the obtained solution $S^*(r_p, \varphi_q, t_m)$ by a factor, characterizing the influence of the gradient pulses (*14*):

$$S(r_p, \varphi_q, t_m) = S^*(r_p, \varphi_q, t_m) \exp(i\gamma g(t_m) r_p \cos(\varphi_q)). \quad [11]$$

## SOFTWARE IMPLEMENTATION

The presented two-dimensional numerical model was implemented in C++ as an extension of the one-dimensional model [9] and inherits all advantages of that model. The time of modelling for particular two-dimensional configurations as given under Results is based on calculations on a Pentium III 550 MHz. The simulations typically yield an array of magnetization spin density as it develops in time and space for a given value of the pulsed field gradient amplitude. Several of these arrays can be compressed into a two-dimensional data set, containing the PFG and relaxation development of the entire system. Random noise was generated during the simulations to avoid fitting problems, so that in all simulations a $S/N$ of 10,000 was reached.

## RESULTS AND DISCUSSION

### Comparison with Other Models

Several computations have been performed to show the correspondence between the presented numerical model and a number of analytically solved models that were published earlier. Although spatial information is available as output of the model, all results shown here are based on the overall decay curves.

We started with a simulation of multiexponential relaxation behavior in the well-known Brownstein–Tarr model (*26*) for a planar and a cylindrical system, without gradient pulses. According to their theory, multiexponential relaxation arises as a consequence of an eigenvalue problem associated with the size and shape of a cell with biologically relevant dimensions; the intensity and decay times of these exponentials can be calculated from the analytical equations. To model the Brownstein–Tarr system, we simulated a single planar or cylindrical compartment with a radius $R_1 = 25\ \mu$m, a diffusion coefficient $D_1 = 2 * 10^{-9}$ m$^2$/s, and an intrinsic relaxation time of 2 s. The relative permeability $M = \rho_1 R_1 / D_1$ of the boundaries was varied between $M = 0.001$ and $M = 1000$. The data were fitted with SPLMOD (*27*), using five discrete exponentials, of which the largest three are plotted in Fig. 2 (symbols). Modelling using 3000 time steps, 500 space steps, and 90 angle steps took approximately 12 minutes. The results show an excellent agreement between the Brownstein–Tarr theory (lines) and our first

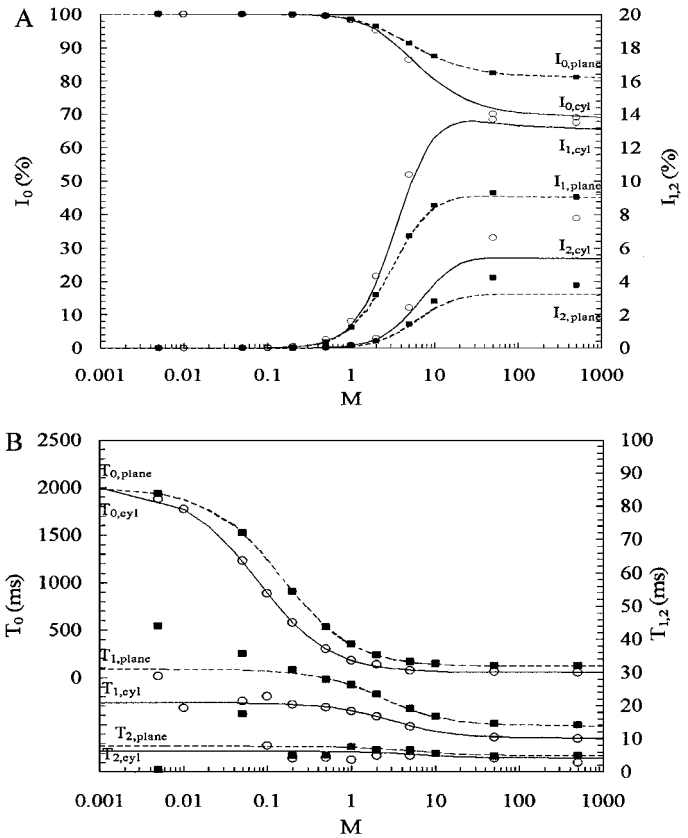


**FIG. 2.** (A) Relative intensity of the first three modes of relaxation as a function of the relative membrane permeability $M = \rho_1 R_1 / D_1$. The Brownstein–Tarr results are depicted as lines (striped for the planar and solid for the cylindrical geometry), whereas our results are plotted with square symbols for the planar geometry, and open circles for the cylindrical geometry. Note the change of scale for the $I_1$ and $I_2$ curves. (B) Decay time of the first three modes of relaxation.

exponential ($I_0$, $T_0$). The second and third components correspond well to the theory for higher intensities. For very low intensities of these components ($M < 0.5$), the relaxation times show some deviations due to fitting errors.

The results of the PFG part of the simulations were verified by comparing them with the Callaghan model (*19*), which describes spin behavior within a confined compartment with closed or permeable boundaries. This model uses a narrow pulse approximation, which was approached by using a very short gradient pulse ($\delta = 0.1$ ms) with a high gradient strength. The simulated system was again a single compartment with a closed or partially permeable boundary ($D_1 = 2 * 10^{-9}$ m$^2$/s, $R_1 = 20\ \mu$m, and $\rho_1 = 0$ or $\rho_1 = 2 * R_1 / D_1$). Relaxation was eliminated by defining infinitely large intrinsic $T_2$ values. Echo attenuation plots obtained by the Callaghan model (solid line) and the present one (symbols) are shown in Fig. 3, for planar (A, B) and cylindrical geometries (C, D) and open (A, C) or closed boundaries (B, D). The echo attenuation is plotted as a function of $(2\pi)^{-1}\gamma g \delta * R_1$. Expressed in multiples of $R_1^2 / D_1$, the observation time $\Delta$ is respectively 0.2, 0.5, 1.0, or 2.0. The results clearly show that our model

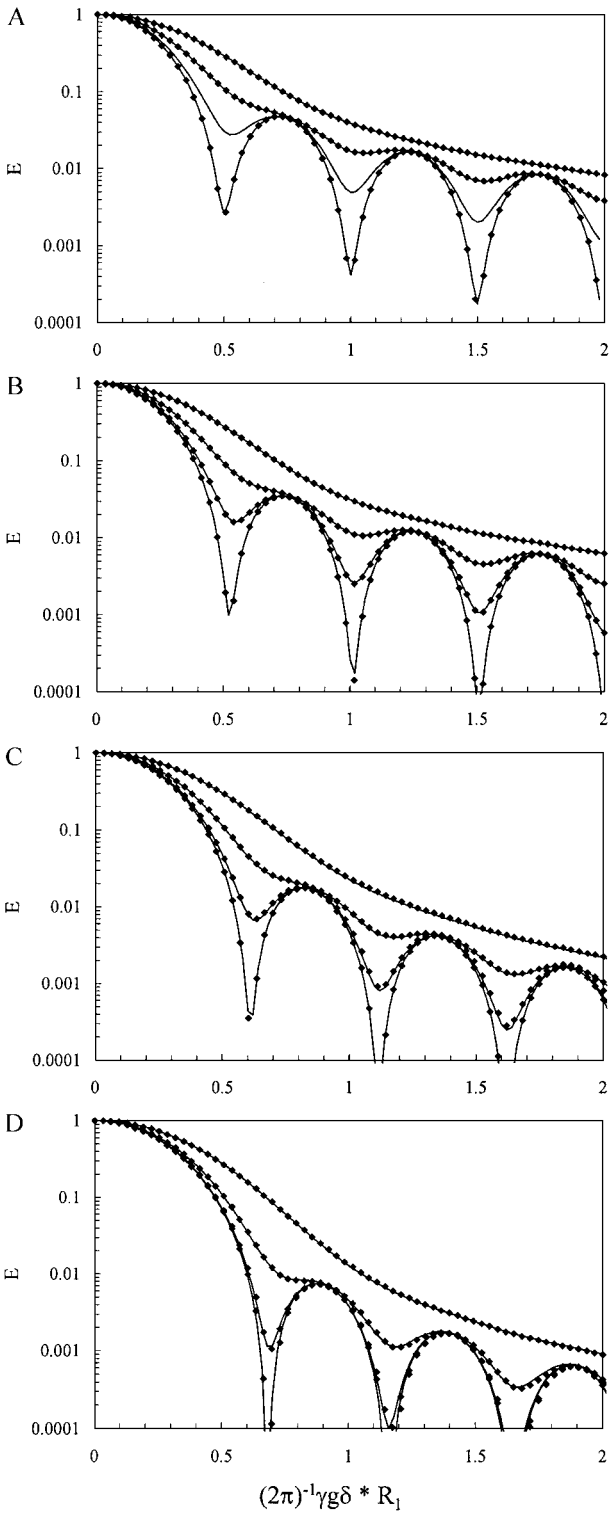


**FIG. 3.** Signal attenuation plots of the Callaghan model (lines) and the present model (symbols) for a one-compartment system. Expressed in multiples of $R_1^2/D_1$, the observation time $\Delta$ is respectively 0.2, 0.5, 1.0, or 2.0 from bottom to top. (A) Planar geometry and fully reflective membranes. (B) Planar geometry and partially permeable membranes ($\rho_1 R_1/D_1 = 2$). (C) Cylindrical geometry and fully reflective membranes. (D) Cylindrical geometry and partially permeable membranes ($\rho_1 R_1/D_1 = 2$).

corresponds excellently to the Callaghan model. Calculation time was 9 minutes when using 64 gradient steps, 400 space steps, and 36 angle steps.

### Effect of Cylindrical Geometry

Molecular motion within multicompartment systems (Fig. 4A) as (plant) cells or porous media will not only depend on the radius of these compartments, but in the cylindrical case also on the probability to circumvent a diffusion barrier by two-dimensional diffusion, i.e., the chance that spins in the outer compartment diffuse from one side of the system around the inner compartment to the other side of the system without passing membranes and the inner compartment. Hence, it is useful to have an understanding of the impact of the geometry on the diffusion and relaxation properties of the system. Therefore, restricted diffusion in a two-dimensional model consisting of concentric cylinders is compared with a one-dimensional system consisting of plan parallel barriers. The simulation of the echo attenuation was done in 16 PFG steps, a typical number for an experimental data set.

First, we compared two systems with cylindrical and planar geometries as shown in Fig. 4A. Both of them consist of two compartments with fully reflective walls. The inner compartment contains no initial magnetization. The diffusion coefficient of the outer compartment is $D_2 = 1 * 10^{-9}$ m$^2$/s and its width $R_1 = R_2$, where $R_1$ is the radius of the inner compartment. For the moment it was assumed that no relaxation occurred in either compartment. The resulting data set was

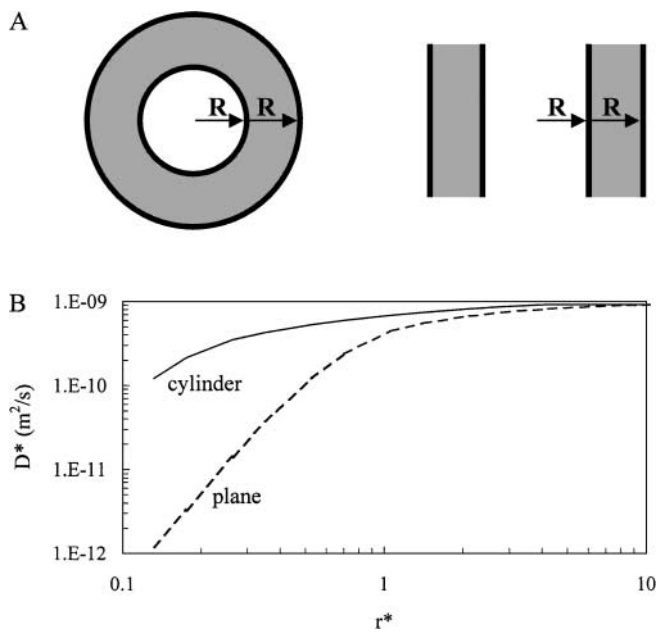


**FIG. 4.** (A) Cylindrical and planar geometries of the examined system. (B) Apparent diffusion coefficient $D^*$ as a function of the relative length of the outer compartment $r^*$ for cylindrical (solid line) and planar (dashed line) geometries (membranes are fully reflecting).

fitted with a single exponential. The dependence of the apparent diffusion coefficient ($D^*$) in the planar and cylindrical configurations on the relative length of the outer compartment $r^* = R_2/(2\sqrt{2D_2(\Delta - \delta/3)})$ is presented in Fig. 4B for $\Delta = 18$ ms and $\delta = 5$ ms. It is clear that especially for small values of $r^*$, the cylindrical configuration provides a less restricted geometry for diffusion than the planar one. The reason for this is that spin-bearing molecules can freely move along the angle axis, and the maximum displacement is only determined by the outer wall at an effective radius $2R_2$. When the relative length $r^*$ increases and diffusion in planar compartment becomes less restricted, the difference between the apparent diffusion coefficients for both geometries gradually disappears and $D^*$ approaches the intrinsic diffusion coefficient.

When the internal membranes of these two-compartment systems become semipermeable, the properties of the "empty" compartment start to play a role as well. We simulated the configurations where either the inner compartment (Fig. 5A(I)) or the outer compartment (Fig. 5A(II)) contains magnetization. For both configurations the ratio $r^*$ equals 1.05, with $R_1 = R_2 = 12$ $\mu$m. The diffusion coefficients are for the inner compartment ($D_1$) $2 * 10^{-9}$ m$^2$/s, and for the outer compartment ($D_2$) $1 * 10^{-9}$ m$^2$/s. All these values are reasonable for a plant cell. In Fig. 5B, the dependencies of the apparent diffusion coefficient $D^*$ on the relative membrane permeability $M$ are shown, for the planar (dashed line) and cylindrical (solid line) geometry. When the outer compartment contains magnetization, an increase in relative permeability causes an increase of both apparent diffusion coefficients, though for the planar case this phenomena is more pronounced. This is because the restriction effects are stronger in the planar system when $M$ is small, as was already shown in Fig. 4B. When the inner membrane becomes more permeable, the differences between the two systems almost disappear.

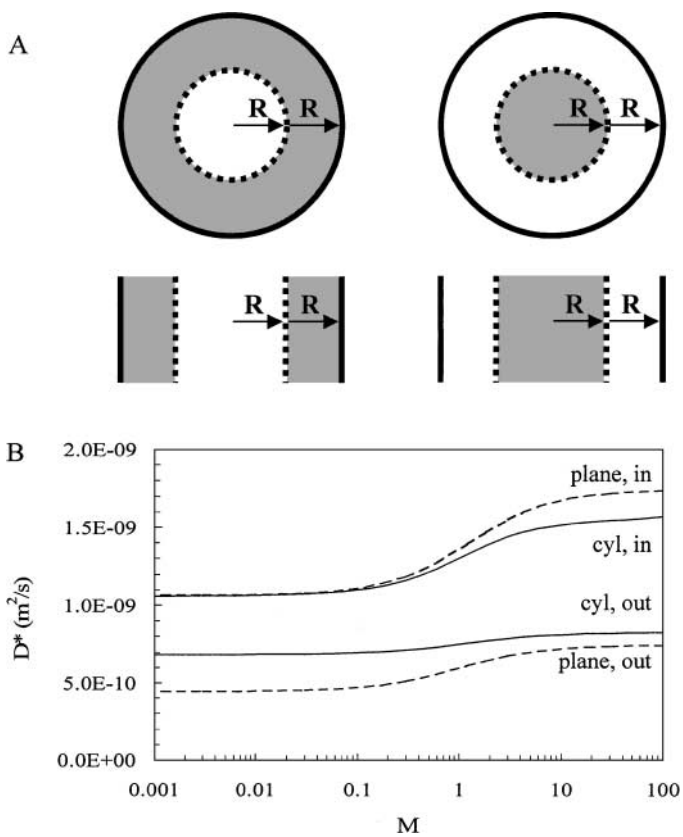


**FIG. 5.** (A) Cylindrical and planar geometries of two examined systems. (B) Apparent diffusion coefficient $D^*$ as a function of the relative membrane permeability $M$ for cylindrical (solid line) and planar (dashed line) geometries. The subscripts *in* and *out* are used to distinguish the inner and outer compartment, respectively.

For the second configuration (Fig. 5A(II)), the parameters remain the same, only now the inner compartment contains magnetization. In this case the apparent diffusion coefficient $D^*$ increases for both cylindrical and planar geometries (Fig. 5B(II)), but the plateau value for high $M$ is lower for the cylindrical geometry. In this case complete exchange between the two compartments occurs, resulting in a lower $D^*$ for the cylinder due to the larger volume of the outer compartment.

In experimental multicompartment geometries, as, for example, plant cells, usually all spins are excited, so all compartments contain magnetization. Such a system is the superposition of the two configurations examined above (Fig. 6A). Now clearly the resulting diffusion attenuation decay shows multiexponential behavior. Hence, a biexponential fit was used to analyze the data (*13*). It should be mentioned that a comparison of cylindrical and planar geometries for such a system is not absolutely correct, because the contribution of the magnetization from each compartment to the whole magnetization is not identical for different geometries, i.e., the ratio of the contributions from the outer and inner compartments equals 1 in the planar case and 3 in the cylindrical case.

For a closed membrane ($M = 0$) the two fitted components for the combined system should correspond to the separate apparent diffusion coefficients in Fig. 5B. As one can see from Figs. 6B and 6C, neither the diffusion coefficients nor the amplitude of these components agree to what is expected from Fig. 5B. The reason is that the diffusion attenuation is not strictly biexponential, but multiexponential, as the diffusion behavior of the spins is not the same for all positions within the compartments. Therefore, the results in Fig. 6 correspond to the best fit of the diffusion attenuation, but the values no longer correspond to the true intensities and apparent diffusion coefficients in the system. The consequence for experimental data is that multiexponential analysis of diffusion behavior cannot freely be related to the geometrical parameters of the system.

Experimentally, additional parameters as $T_2$ can be used to provide extra contrast to extract physiologically relevant parameters (*13*). This was simulated for these two-compartment systems by introducing an intrinsic relaxation time of 2 s for the inner compartment, and 0.2 s for the outer one, which are reasonable values for a plant cell (*2*). The parameters for these

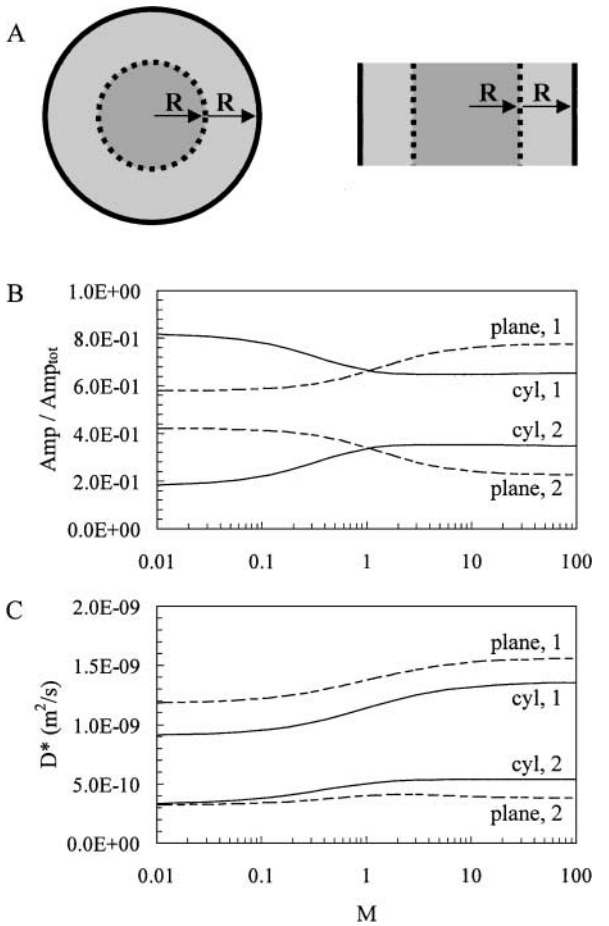


**FIG. 6.** (A) Cylindrical and planar geometries of the examined system. (B) Amplitude of the fractions divided by the input value as a function of the relative membrane permeability $M$ for cylindrical (solid line) and planar (dashed line). (C) Apparent diffusion coefficient $D^*$ as a function of the relative membrane permeability $M$ for cylindrical (solid line) and planar (dashed line) geometries.

simulations were chosen as in an experimental PFG-CPMG experiment (DARTS) (*13*), i.e., a PFG part of 16 gradient steps, combined with an echo train of 1000 echoes with an interecho time of 5 ms. Calculations took 15 minutes for 120 space steps, 36 angle steps, 16 gradient steps, and 1000 time steps. The resulting two-dimensional data sets were fitted with a coupled fitting routine; first a biexponential fit was done on the relaxation part with SPLMOD, and next the fitted intensities were used to fit the corresponding diffusion fractions.

For very small $M$ values, the fractions of the two components and the corresponding $T_2$ are equal to the input parameters ($T_2 = 2$ s and 0.2 s; amplitude = 1 : 1 for the planar and 1 : 3 for the cylindrical case) and $D^*$ corresponds to the diffusion coefficients for the separated systems in Fig. 5 (lines in Figs. 7A–7C), in contrast to those in Fig. 6. This clearly shows that the use of $T_2$ information is advantageous for discriminating different fractions in a multicompartment system. When the membrane permeability increased, the relaxation behavior evolved to an

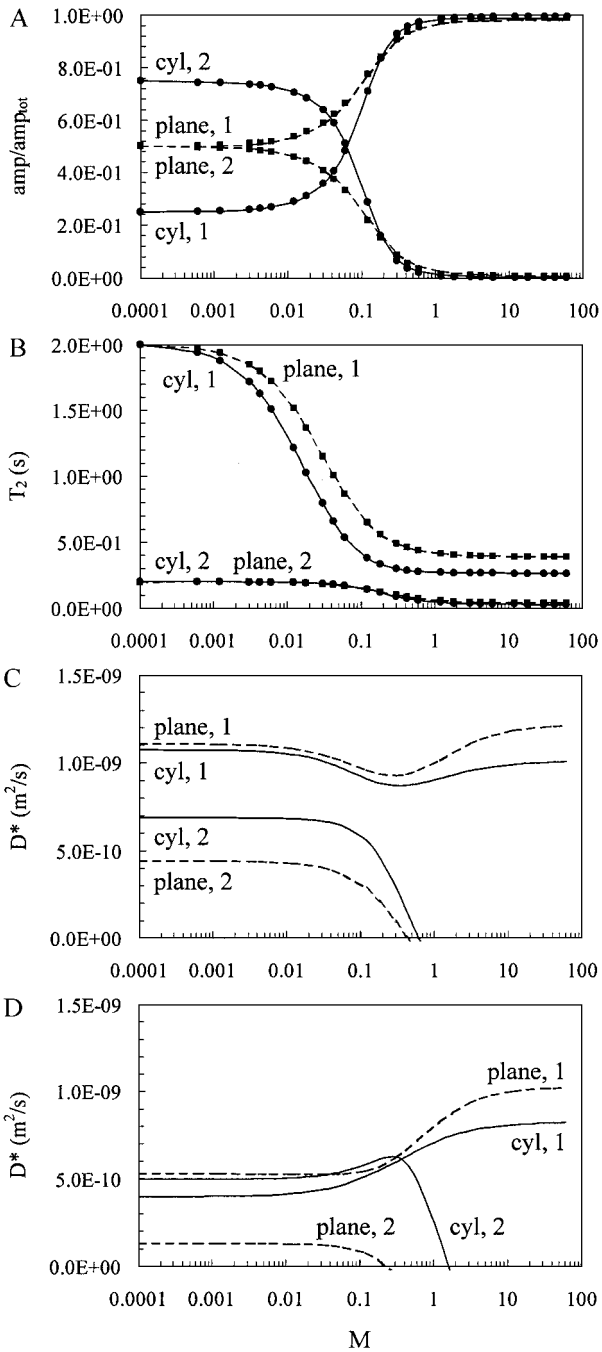


**FIG. 7.** The same system was used as in Fig. 6, but with relaxation behavior. (A) Amplitude of the fractions divided by the input value as a function of the relative membrane permeability $M$ for cylindrical (solid line) and planar (dashed line) for simulations with an diffusion observation time $\Delta = 18$ ms. The results for the simulations with $\Delta = 90$ ms are overplotted with symbols (squares for the planar geometry and circles for the cylindrical geometry). (B) Relaxation time of the fractions. Linestyles and symbols correspond to those in Fig. 7A. (C) Apparent diffusion coefficient $D^*$ for an observation time $\Delta$ of 18 ms. (D) Apparent diffusion coefficient $D^*$ for an observation time $\Delta$ of 90 ms.

almost monoexponential decay, due to complete averaging of the two compartments. The corresponding diffusion coefficients first decrease due to averaging of the two fractions, but start to increase as soon as the relaxation decay becomes monoexponential, and, as expected, the increase is more pronounced for planar geometries. It should be noted that though a multiparameter approach is useful to discriminate compartments separated by a membrane, the fitted parameters amplitude, $T_2$ and $D^*$, are no longer uniquely reflecting the properties of the different compartments when the membrane becomes reasonably permeable ($M > 0.01$). For instance the value of the longest $T_2$ component, originating from the central compartment of the model, becomes strongly dependent on those of the second compartment and the actual membrane permeability.

Figure 7D shows the effect of a longer observation time $\Delta$ (90 ms). The amplitude and $T_2$ fits yield exactly the same results as those for $\Delta = 18$ ms (symbols in Figs. 7A, 7B). The restriction effects on $D^*$, on the contrary, become much more pronounced. For small $M$, all values are decreased, though only slightly in the cylindrical outer compartment (solid line). This is a prominent illustration of the effect of circumvential motion to overcome diffusion restriction, and for $M < 1$ such data sets with varying observation time $\Delta$ can be very useful for discrimination between planar and cylindrical geometries.

## CONCLUSIONS

A numerical model for diffusion and magnetization relaxation behavior in PFG-CPMG NMR experiments has been extended to a two-dimensional system with concentric cylindrical geometry. The results of this model show excellent agreement with published analytical results. As an example of the relevance of a two-dimensional model, the behavior of the apparent diffusion coefficients and relaxation times in a multicompartment system with the properties of a plant cell has been modelled for both a planar and a cylindrical geometry. When the difference in diffusion coefficients is relatively small, supplementary contrast parameters as $T_2$ are needed to unravel the different fractions present. The difference between the obtained values of the apparent diffusion coefficients and the true ones can be explained by the influence of non- or semipermeable membranes (restricted diffusion). This restriction effect is more pronounced for planar systems than for cylindrical ones. Furthermore, the differences in diffusion coefficients between the two geometries become larger for longer observation times. Together, this clearly demonstrates the need for a two-dimensional system to be able to understand experimental results in terms of geometry.

## REFERENCES


1. F. R. E. Fenrich, C. Beaulieu, and P. S. Allen, Relaxation times and microstructures, *NMR Biomed*. **14,** 133–139 (2001).
2. J. E. M. Snaar and H. Van As, Probing water compartment and membrane permeability in plant cells by proton NMR relaxation measurements, *Biophys. J.* **63,** 1654–1658 (1992).
3. Y. Q. Song, S. Ryu, and P. N. Sen, Determining multiple length scales in rocks, *Nature* **406,** 178–181 (2000).
4. H. Van As and D. Van Dusschoten, NMR methods for imaging of transport processes in micro-porous systems, *Geoderma* **80,** 389–403 (1997).
5. D. van Dusschoten, C. T. Mooenen, P. A. de Jager, and H. Van As, Unraveling diffusion constants in biological tissue by combining Carr–Purcell–Meiboom–Gill imaging and pulsed field gradient NMR, *Magn. Reson. Med.* **36,** 907–913 (1996).
6. B. P. Hills and J. E. M. Snaar, Dynamic q space microscopy of cellular tissu, *Mol. Phys.* **76,** 979–994 (1992).
7. P. W. Kuchel and C. J. Durrant, Permeability coefficients from NMR q-space data: Models with unevenly spaced semi-permeable parallel membranes, *J. Magn. Reson.* **139,** 258–272 (1999).
8. P. P. Mitra and P. N. Sen, Effects of microgeometry and surface relaxation on NMR pulsed-field-gradient experiments: Simple pore geometries, *Phys. Rev. B* **45,** 143–156 (1992).
9. E. G. Novikov, D. van Dusschoten, and H. Van As, Modeling of self-diffusion and relaxation time NMR in multi-compartment systems, *J. Magn. Reson.* **135,** 522–528 (1998).
10. J. Pfeuffer, U. Flogel, W. Dreher, and D. Leibfritz, Restricted diffusion and exchange of intracellular water: Theoretical modelling and diffusion time dependence of H-1 NMR measurements on perfused glial cells, *NMR Biomed.* **11,** 19–31 (1998).
11. J. E. M. Snaar and H. Van As, NMR self-diffusion measurements in a bounded system with loss of magnetization at the walls, *J. Magn. Reson. Ser. A* **102,** 318–326 (1993).
12. G. J. Stanisz, J. G. Li, G. A. Wright, and R. M. Henkelman, Water dynamics in human blood via combined measurements of T2 relaxation and diffusion in the presence of gadolinium, *Magn. Reson. Med.* **39,** 223–233 (1998).
13. D. van Dusschoten, P. A. de Jager, and H. Van As, Extracting diffusion constants from echo-time-dependent PFG NMR data using relaxation-time information, *J. Magn. Reson. Ser. A* **116,** 22–28 (1995).
14. T. A. Zawodzinski, T. E. Springer, M. Neeman, and L. O. Sillerud, Diffusion barriers in pulsed-gradient spin-echo NMR microscopy, *Israel J. Chem.* **32,** 281–289 (1992).
15. G. J. Stanisz and R. M. Henkelman, Diffusional anisotropy of T2 components in bovine optic nerve, *Magn. Reson. Med.* **40,** 405–410 (1998).
16. A. Traore, L. Foucat, and J. P. Renou, H-1-NMR study of water dynamics in hydrated collagen: Transverse relaxation-time and diffusion analysis, *Biopolymers* **53,** 476–483 (2000).
17. S. M. Schoberth, N. K. Bar, R. Kramer, and J. Karger, Pulsed high-field gradient in vivo NMR spectroscopy to measure diffusional water permeability in Corynebacterium glutamicum, *Anal. Biochem.* **279,** 100–105 (2000).
18. M. D. Does and J. C. Gore, Compartmental study of diffusion and relaxation measured in vivo in normal and ischemic rat brain and trigeminal nerve, *Magn. Reson. Med.* **43,** 837–844 (2000).
19. P. T. Callaghan, Pulsed-gradient spin-echo NMR for planar, cylindrical, and spherical pores under conditions of wall relaxation, *J. Magn. Reson. Ser. A* **113,** 53–59 (1995).
20. H. Gudbjartsson and S. Patz, NMR diffusion simulation based on conditional random walk, *IEEE Trans. Med. Imag.* **14,** 636–642 (1995).
21. P. Linse and O. Söderman, The validity of the short-gradient-pulse approximation in NMR studies of restricted diffusion: Simulations of molecules diffusing between planes, in cylinders and spheres, *J. Magn. Reson. Ser. A* **116,** 77–86 (1995).

*22.* J. Crank, "The Mathematics of Diffusion," Oxford Univ. Press, Oxford (1975).

*23.* L. van der Weerd, M. A. E. Claessens, T. Ruttink, F. J. Vergeldt, T. J. Schaafsma, and H. Van As, Quantitative NMR microscopy of osmotic stress responses in maize and pearl millet, *J. Exp. Bot.* **52,** 2333–2343 (2001).

*24.* T. Meis and U. Marcowitz, "Numerical Solutions of Partial Differential Equations," Springer-Verlag, New York (1981).

*25.* P. T. Callaghan, "Principles of Nuclear Magnetic Resonance Microscopy," Clarendon, Oxford (1991).

*26.* K. R. Brownstein and C. E. Tarr, Importance of classical diffusion in NMR studies of water in biological cells, *Phys. Rev. A* **19,** 2446–2453 (1979).

*27.* S. W. Provencher and R. H. Vogel, Regularization techniques for inverse problems in molecular biology, *in* "Numerical Treatment of Inverse Problems in Differential and Integral Equations" (P. Deuflhard and E. Hairer, Eds.), pp. 304–319, Birkhäuser, Boston (1983).